Ceramics-Silikáty 67 (2), 182-188 (2023)
www.ceramics-silikaty.cz doi: 10.13168/cs.2023.0016

PREPARATION AND FERROELECTRIC PROPERTIES OF STRONTIUM-DOPED HYDROXYAPATITE CERAMICS

HONGQUAN ZHANG, QI ZHANG, #JIN WEN, JINGLI YANG

School of Materials Science and Engineering, Wuhan University of Technology, Wuhan 430070, PR China

#E-mail: wen9888@Hotmail.com

Submitted February 23, 2023; accepted March 29, 2023

Keywords: Strontium doping, Hydroxyapatite, Ferroelectric properties, Remnant polarization intensity

Strontium-doped hydroxyapatite ceramics with good ferroelectric properties were prepared using 5 % bioactive phosphate glass as an additive at 700 °C in this paper. XRD, FTIR, SEM analyses and a ferroelectric tester were used to analyse the crystal structure, phase composition, microstructure and ferroelectric properties of the prepared ceramics. The results revealed that substitution of Ca^{2+} by Sr^{2+} in the HA lattice would lead to an increase in its lattice parameters and a decrease in crystallinity. Moreover, the lattice distortion and the increase in the electric dipole moment caused by the Sr^{2+} doping enhanced the ferroelectric properties of the Sr-HA ceramics. Increasing the density of the samples could enhance their ferroelectric properties. The remnant polarisation intensity increased from 0.0156 μC·cm-2 to 0.0728 μC·cm-2, the maximum polarisation intensity increased from 0.1210 μC·cm^{-2} to 0.1628 μC·cm^{-2}.

INTRODUCTION

Artificial bone repair materials are an important source of bone repairs due to the increasing demands for the restoration and replacement of bones damaged by fracture and diseases [1]. Hydroxyapatite (HA) has a chemical composition similar to that of vertebrate bones and has been widely used in biomedical fields owing to its excellent bioactivity, biocompatibility and bone conductivity [2]. However, its low dissolvability and degradation rate under normal physiological conditions and poor mechanical properties greatly delays the growth and regeneration of natural bone [3]. Therefore, research and development of HA materials with good biological and mechanical properties have always been a concern by both material and clinical researchers.

Piezoelectric biomaterials have been found to show a piezoelectric effect similar to that of human bones, they can generate polarisation and electrical charges on their surface after being implanted into the human body, and the electrical signal generated can effectively stimulate the regeneration of bone tissue and promote bone healing [4]. Therefore, the piezoelectric biomaterials have gradually attracted the attention of biomedical researchers in recent years. Up to now, barium titanate based piezoelectric ceramics, polarised hydroxyapatite and polylactic acid, etc. have been used for bone repairs [5]. Although barium titanate has the advantages of a high dielectric constant, good mechanical properties and low attrition, its biological inertness greatly impairs the cell adhesion, proliferation and other physiological activities. Moreover, the high cytotoxicity of titanium and barium ions is harmful to human health [6]. As for polylactic acid (PLA) materials, despite having good biocompatibility and piezoelectric properties, and being rapidly degraded and absorbed in vivo, its low mechanical strength hardly meets the requirements of fixation and treatment for bone injuries [7]. Polarised hydroxyapatite has recently been found to be able to keep static electricity for a long time, and continuously release enough electrostatic energy to promote new bone formation [8]. Nevertheless, its poor ferroelectric effect cannot significantly promote the growth of bone tissue. Thus, the development of HA with excellent ferroelectric properties has attracted the attention more and more experts.

Generally, biological apatite is a calcium-deficient hydroxyapatite containing a variety of ion substitution [9]. Ion doping could affect the thermal stability, mechanical properties, solubility and surface activity of the material by changing its crystal structure, phase composition and micro morphology [10], but also greatly improves the biological properties of the HA implants [11]. In the case of an Sr^{2+} substitute for Ca^{2+} in HA crystals, Sr^{2+} doping can promote the proliferation of osteoblasts and inhibit the activity and proliferation of osteoclasts [12]. Although researchers have undertaken a great deal of studies on the structure and biological properties of metal ion-doped HA, there are few literature pieces on the ferroelectric properties of metal ion-doped HA. Recently,

the ferroelectric properties of hydroxyapatite have been reported to be related to its degree of electric polarisation. Al-Wafi et al. [13] claimed that strontium doping could change the electrical and dielectrical properties of HA ceramics by changing their electrode and dipole moment, and their dielectric constant increased with the Sr^{2+} doping amount, while the remnant polarisation intensity generally first increased and then decreased. AlHammad [14] found that boron doping could reduce the electric dipole moment of HA, and also inhibited the electrode of HA to a certain degree. The dielectric constant of HA ceramics decreased with an increase in the boron doping amount, and their remnant polarisation intensity showed a non-linear trend. However, they have not systematically studied the influence of the crystal structure, phase composition, density and other factors of ion doped HA ceramic materials on the ferroelectric properties of HA based biomaterials.

Therefore, to prepare HA with excellent ferroelectric and biological properties, strontium ion-doped HA ceramic materials were calcined using HA powders containing various strontium ion contents and phosphate bioactive glass as additive at 700 °C. The effects of the crystal structure, phase composition and microstructure on the ferroelectric properties of HA were studied here. It would be expected to provide a theoretical basis for obtaining HA bioceramics with excellent ferroelectric and biological properties.

EXPERIMENTAL

Preparation of the strontium-doped HA powders and bioglass

The strontium-doped HA powders were prepared by a homogeneous precipitation method from a solution containing 0.5 mol·l^{-1} $Ca(NO_3)_2 \cdot 4H_2O$, 0.5 mol·l^{-1} $Sr(NO_3)_2$ and 0.3 mol·l^{-1} $NH_4H_2PO_4$ (all AnalaR grade, Sinopharm Chemical Reagent Co., Ltd., Shanghai, China) according to the (Ca+Sr)/P molar ratio of 1.67. After drying in an oven at 120 °C for 1-2 h, the powders were ground through a 300-mesh sieve for further use. The phosphate bioglass was prepared by a melt method using 15–18 mol. % $CaCO_3$, 15 mol. % SiO_2, 6 mol. % MgO, 5 mol. % ZnO, 20–23 mol. % $NH_4H_2PO_4$, and 12 mol. % Na_2CO_3 (all AnalaR grade, Sinopharm Chemical Reagent Co., Ltd., Shanghai, China) at 1100 °C for 2 h. After quenching, the bioglass was dried and ground through a 300-mesh sieve for further use.

Preparation of the strontium-doped HA ceramics

The powder mixture containing the strontium-doped HA powders and 5 wt. % phosphate bioglass were evenly wet-mixed using analytical ethanol. After drying, they were granulated with a 3 wt. % polyvinyl alcohol (PVA) binder, and dry-pressed to form disk samples of ø 12 × 1.0 mm at 80 MPa, and then processed using a cold isostatic pressing machine (LDJ320/700-400, Sichuan Aviation Industry Chuanxi Machinery Factory, China) at a cold isostatic pressure 200 MPa for 5 minutes. Subsequently, the prepared samples were calcined from room temperature to 600 °C at a heating rate of 5 °C·min^{-1} and remained there for 1 h, then were continued to be heated to 700 °C at a heating rate of 5 °C·min^{-1} and remained there for 0.5 h.

Characterisation

The phase compositions of the products were characterised by X-ray powder diffraction (XRD) (Empyrean, Malvern PANalytical, Holland) and Fourier-transform infrared spectroscopy (FTIR) (Nexus, Nicolet, USA). The morphology and microstructure were observed by scanning electron microscopy (SEM) (QUANTA FEG 450, FEI, China) and the electric hysteresis loop of the ion-doped HA ceramics was tested by a ferroelectric tester (Precision Workstation, Radiant, USA).

The crystallinity degree of the Sr-HA, corresponding to the fraction of the crystalline phase present in the examined volume, was evaluated by the formula [15]:

$$Xc = 1 - (V_{112/300}/I_{300}) \quad (1)$$

where $V_{112/300}$ is the intensity of the hollow between the (112) and (300) peaks and I_{300} is the intensity of the (300) peak in the corresponding XRD pattern.

RESULTS AND DISCUSSION

Phase composition of the Sr-HA ceramics

Figure 1 shows the XRD pattern of the HA and Sr-HA ceramics prepared at 700 °C. When the Sr^{2+} doping contents are ≤ 15 mol. %, all the XRD peaks well matched those in the JCPDS PDF 9-432 diffraction

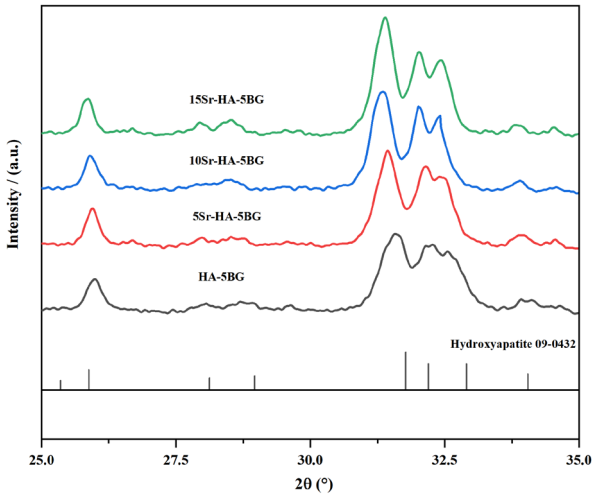

Figure 1. XRD pattern of the HA and Sr-HA ceramics.

pattern for synthetic HA. However, the diffraction peak shifted to the left, and became broader and broader with the increase in the Sr^{2+} doping, which is consistent with the findings of Wen [16] and Geng [17]. The difference in the radius of the doped metal ions and the Ca ions of the HA crystals has been proven to be the main reason that causes the shift in the XRD diffraction peak of HA and the different substitution positions of the doped ions in the crystal, but also has a great influence on the phase, morphology, crystallinity and thermal stability of HA [17]. In addition, according to the Bragg equation $\lambda = 2d \cdot \sin \theta$, when the wavelength λ of the X-rays remains constant, the diffraction angle θ would decrease with the increase in the lattice plane spacing d. For Sr-HA, because the radius of Sr^{2+} (0.118 nm) is slightly larger than that of Ca^{2+}(0.099 nm), the substitution of Ca^{2+} by Sr^{2+} would give rise to a lattice distortion and an increase in the lattice plane spacing, leading to the diffraction pattern of Sr-HA to shift to a lower angle.

Table 1 shows the changes in the lattice parameters and crystallinity of the HA phase in the Sr-HA ceramics. The lattice parameters a and c increased gradually from 9.4758 to 9.5402 Å, and from 6.8510 to 6.8845 Å, respectively, but the crystallinity decreased with the increase in the Sr^{2+} doping, which coincides with previous reports. Baravelli [18] et al. pointed out that the cations similar in size and charges to Ca^{2+} could easily exchange with Ca^{2+}, among them, metal ions with a smaller radius were preferentially adsorbed at the Ca(I) position and those with a larger radius favoured to be adsorbed at the Ca(II) position. Based on this principle, Sr^{2+} has a slightly larger radius than Ca^{2+}, and would preferentially occupy the both the Ca(I) and Ca(II) positions, resulting in an increase in the lattice parameters. Li et al. [19] found that the length and width of Sr-HA crystals doped with 0.3 % - 1.5 % Sr^{2+} also increased, where only a slight change in the crystallinity occurred. However, when the Sr^{2+} doping content reached 15 %, the crystallinity of the Sr-HA significantly reduced. Geng et al. [17] found that the crystallinity of the Sr-HA decreased significantly when the Sr^{2+} doping reached 20 %, which was mainly because the Sr^{2+} doping led to a greater distance between the Sr-hydroxyl groups than the Ca-hydroxyl groups, giving rise to the lattice distortion and disruption of the specific hexagonal structure of HA. As shown in Table 1, the crystallinity of the Sr-HA ceramics obtained here was between 30.10 % and 60.08 %, coinciding with the literature. Excessive Sr doping disrupted the symmetry of the HA crystal structure, giving rise to a change in the crystal composition and a reduction in the crystallinity.

Figure 2 shows the FTIR spectra of the HA and Sr-HA ceramics. The characteristic stretching and bending motions of the phosphate group at 1087, 1042, 963, 604, and 563 cm^{-1} and the stretching mode of the hydroxyl group at 3576 and 633 cm^{-1} were clearly visible. The absorption peaks appeared at 3441 cm^{-1} and 1634 cm^{-1} were mainly caused due to the adsorption of H_2O. In addition, the absorption peak of the $P_2O_7^{4-}$ group was also found to appear at 946 cm^{-1}, indicating that a small amount of pyrophosphate occurred in the sintering process. Zhang et al. [20] pointed out that HPO_4^{2-} was easy to condense and produced $P_2O_7^{4-}$ when the calcium defective HA was calcined in a temperature range of 250–720 °C. Because the Sr-HA synthesised here was a calcium defective apatite, the appearance of the $P_2O_7^{4-}$ group was mainly caused by the shrinkage of HPO_4^{2-} in the crystal to pyrophosphate during heating.

In addition, as shown in Figure 2, the infrared absorption peaks assigned as the $P_2O_7^{4-}$ and OH^- groups weaken with an increase in the Sr^{2+} doping. When the Sr^{2+}

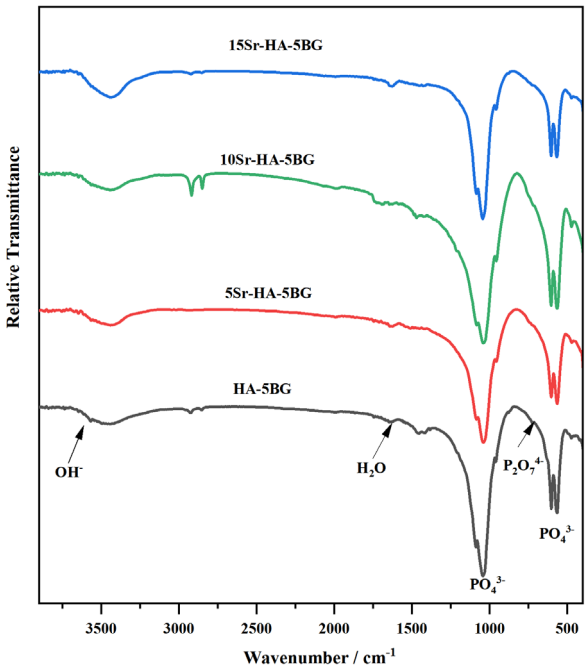

Figure 2. FTIR spectra of the HA and Sr-HA ceramics.

Table 1. Lattice parameters and crystallinity of the HA phase in the Sr-HA ceramics.

Samples	Sr^{2+} doping concentration (%)	Lattice parameters of HA		Crystallinity (%)
		a = b/nm mean ± SD	c/nm mean ± SD	
HA-5BG	0	9.4758 ± 0.0072	6.8510 ± 0.0036	60.08
5Sr-HA-5BG	5	9.5159 ± 0.0073	6.8564 ± 0.0031	42.36
10Sr-HA-5BG	10	9.5209 ± 0.0068	6.8827 ± 0.0111	30.10
15Sr-HA-5BG	15	9.5402 ± 0.0076	6.8845 ± 0.0033	

doping content was more than 10 wt. %, no $P_2O_7^{4-}$ group could be detected, which indicated that $P_2O_7^{4-}$ might have started to react with OH^- due to its low crystallinity and high calcium deficiency.

Ferroelectric properties of the Sr-HA ceramics

Figure 3 shows the hysteresis loop diagrams and ferroelectric characteristic parameters of the Sr-HA ceramics with or without the bioglass additives. All the samples could withstand the external electric field of 0–0.8 KV·mm^{-1}, showing a single hysteresis loop similar to that of normal ferroelectrics. As shown in Figure 3a, with an increase in the Sr^{2+} doping, the remnant polarisation intensity of the Sr-HA prepared without adding bioglass gradually increased from 0.0115 μC·cm^{-2} to 0.0626 μC·cm^{-2} and the maximum polarisation intensity P_{max} increased from 0.1165 μC·cm^{-2} to 0.1575 μC·cm^{-2}, gradually showing enhanced ferroelectric properties. For the samples with 5 % bioglass (see Figure 3b), the remnant polarisation intensity of the Sr-HA increased from 0.0156 μC·cm^{-2} to 0.0728 μC·cm^{-2}, the maximum polarisation intensity Pmax increased from 0.1210 μC·cm^{-2} to 0.1628 μC·cm^{-2}, indicating that an appropriate amount of bioglass could be used as an additive to enhance the ferroelectric properties of HA ceramics.

Figure 3c shows the variation of the ferroelectric characteristic parameters, such as the maximum polarisation intensity P_{max}, remnant polarisation intensity P_r and coercive electric field intensity E_c in the hysteresis loop with the Sr^{2+} doping contents. For the samples with 5 % bioglass, the coercive electric field intensity E_c linearly increased approximately, increasing from 0.0313 KV·mm^{-1} to 0.3184 KV·mm^{-1}, the electric field intensity required for domain flipping also increased. The maximum polarisation intensity P_{max} gradually increased from 0.1210 μC·cm^{-2} for the undoped sample to 0.1628 μC·cm^{-2}. At the same time, the remnant polarisation intensity Pr also increased from 0.0156 μC·cm^{-2} to 0.0728 μC·cm^{-2}, indicating that the Sr^{2+} doping had a good stabilising effect on the ferroelectric long-term programme of HA. Considering the changes in the lattice parameters (Table 1), both the lattice parameters a and c gradually increased with the increase in the Sr^{2+} doping, the lattice distortion and the increase in the electric dipole moment caused by the Sr^{2+} doping were speculated to be intimately related with the enhancement of the ferroelectric properties of the Sr-HA ceramics materials.

Terra et al. [21] studied the crystal structure of Sr^{2+} doped hydroxyapatite using a first-principle modelling combined with experimental methods, and pointed out that Sr^{2+} doping could cause the lattice distortion of HA crystals and the degree of lattice disorder and the loss of OH would increase with an increase in the Sr^{2+} doping. Bigi et al. [22] refined the crystal structure of strontium ion doped HA by the Rietveld method, and claimed that strontium ions would preferentially occupy the Ca(I) position when its doping concentration was low. As the Sr^{2+} doping concentration increased, it would preferentially occupy the Ca(II) position, and the degree of lattice distortion caused by occupying the Ca(II) position became greater than that of the Ca(I) position. Additionally, Liu et al. [23] also pointed out that the Ca-O bond length was less than the Sr-O bond length in the Sr-HA crystal structure, the Ca-O bond energy was greater than the Sr-O bond energy, which led to the symmetry of the crystal structure decreasing after Sr^{2+} replaced Ca^{2+}, and the higher the strontium content, the more unstable the group was. Moreover, Sun et al. [24] found that Sr^{2+} doping would cause the lateral rotation of PO_4^{3-} around Sr^{2+} when Sr^{2+} occupies the Ca(II) position. Therefore, it can be inferred that the enhancement of the ferroelectric polarisation intensity of the samples may be due to the changes in the cation-oxygen bond distance, cation-cation distance, bond length and torsion angle in the HA cells caused by the difference in the radius of Sr^{2+} and Ca^{2+}. The Sr^{2+} occupation on the positions of Ca(I) and Ca(II) of the HA lattice would lead to the rotation of PO_4^{3-} around Sr^{2+}, the decrease in the cell symmetry and the increase in the electric dipole moment of the HA crystal cell. Therefore, the ferroelectric properties of Sr-HA ceramics were enhanced under the action of an external electric field.

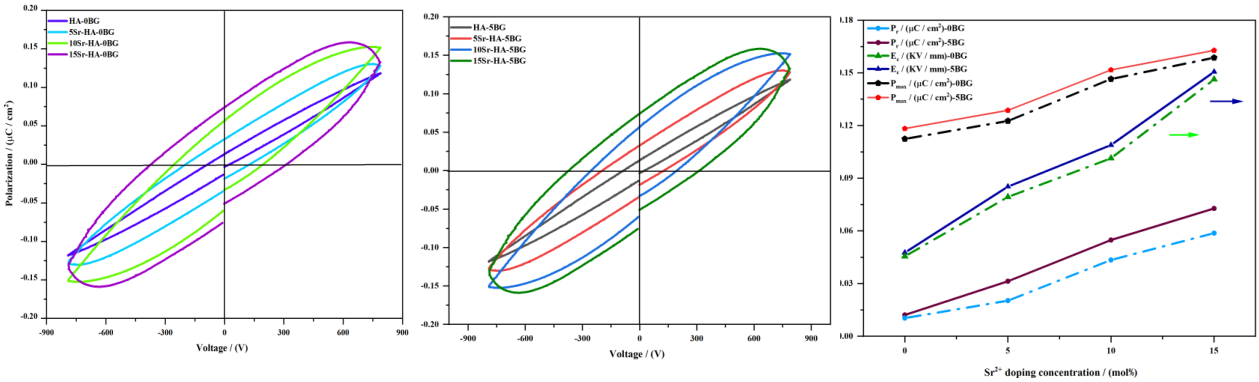

Figure 3. Hysteresis loop diagrams and ferroelectric characteristic parameters of the Sr-HA ceramics.

Effect of the densification degree on the ferroelectric properties of Sr-HA ceramics

Figure 4 shows the SEM images of Sr-HA ceramics with different Sr^{2+} doping contents. The grain size was small and uniformly distributed in the fractured surface. Nevertheless, although the grain size did no show an obvious change with the increase in the Sr^{2+} doping, grain agglomeration occurred. In addition, it can be seen from the images that there were certain pores in the Sr-HA ceramics. The existence of pores would lead to an increase in the porosity.

Table 2 shows the physical and ferroelectric properties of the samples obtained using different forming methods. The densification degree of the Sr-HA ceramics showed obvious effects on the physical and ferroelectric properties. The porosity of the Sr-HA ceramics formed by cold isostatic pressing was between 26.40 % and 44.28 %, and the remnant polarisation intensity was between 0.0156 $\mu C \cdot cm^{-2}$ and 0.0728 $\mu C \cdot cm^{-2}$. While the porosity of the Sr-HA ceramics formed by simple dry pressing was much higher than that of the cold isostatic pressing samples, showing a porosity of 40.53 % to 52.85 % and a remnant polarisation intensity of 0.0134 $\mu C \cdot cm^{-2}$ to 0.0720 $\mu C \cdot cm^{-2}$. Meanwhile, the

Table 2. Comparison of the parameters formed by the different methods.

Method	Samples	Porosity (%)	Volume density ($g \cdot cm^{-3}$)	P_r ($\mu C \cdot cm^{-2}$)	P_{max} ($\mu C \cdot cm^{-2}$)	E_c ($KV \cdot mm^{-1}$)
Cold isostatic pressing	HA-5BG	26.40	1.90	0.0156	0.1210	0.0313
	5Sr-HA-5BG	39.27	1.74	0.0308	0.1287	0.1367
	10Sr-HA-5BG	44.28	1.81	0.0626	0.1517	0.2025
	15Sr-HA-5BG	40.11	2.29	0.0728	0.1628	0.3184
Simple dry pressing	HA-5BG	49.00	1.61	0.0134	0.1184	0.0432
	5Sr-HA-5BG	45.32	1.56	0.0265	0.1225	0.1553
	10Sr-HA-5BG	52.85	1.48	0.0512	0.1496	0.2316
	15Sr-HA-5BG	40.53	1.55	0.0720	0.1597	0.3209

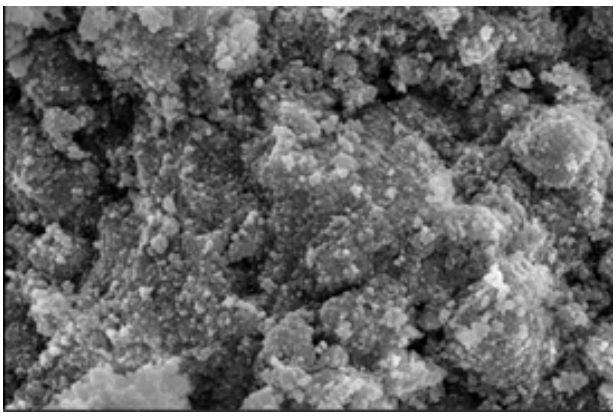

a) HA

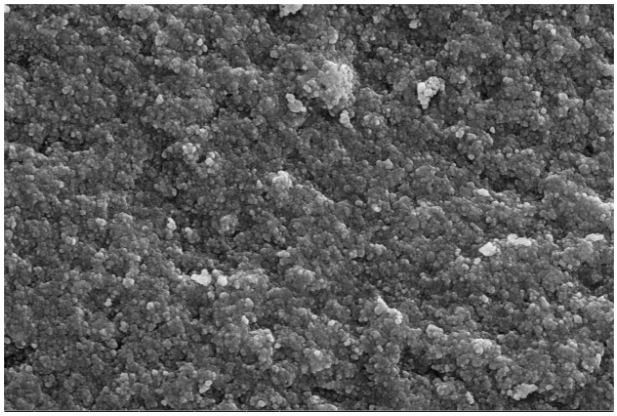

b) HA-5BG

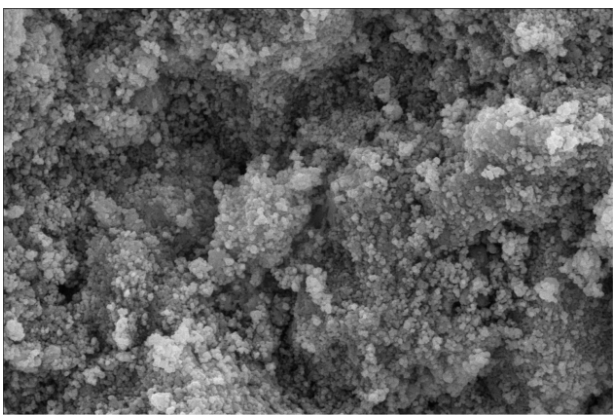

c) 5Sr-HA

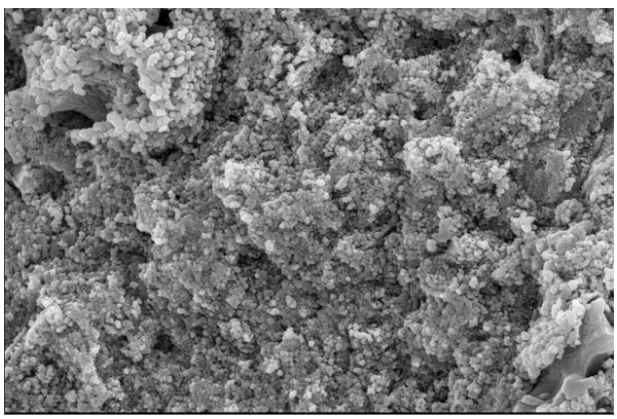

d) 5Sr-HA-5BG

Figure 4. SEM images of the HA and Sr-HA ceramics.

maximum polarisation intensity of the Sr-HA ceramics formed by cold isostatic pressing were also higher than those of the Sr-HA ceramics formed by simple dry pressing, but the coercive electric field intensity formed by cold isostatic pressing were lower than those of the Sr-HA ceramics formed by simple dry pressing. The results indicated that the higher the porosity, the worse the ferroelectric properties of Sr-HA ceramics.

The effect of the porosity of the ceramic materials on their remnant polarisation and ferroelectric properties have been studied in recent years. Zeng et al. [25] reported that the porosity, pore size and pore shape of porous lead zirconate titanate (PZT) ferroelectric ceramics showed obvious effects on their mechanical and ferroelectric properties. Their coercive electric field intensity enhanced with an increase in the porosity. When the external electric field was exerted to the porous ceramics, a large part of the voltage would be applied to the pores, only small voltage was applied on the ceramics; meanwhile, stress concentration around the hole would hinder the domain wall movement, leading to a larger electric field being needed to make the porous ceramic domain wall turn. Zhang et al. [26] also pointed out that the remnant polarisation intensity Pr decreased with an increase in the porosity, but the coercive electric field intensity increased. Padurariu [27] and Gheorghiu [28] attributed the decrease of P_s and P_r to the amount of the active phase and the average electric field applied on the active phase was lower than that of the applied electric field.

As shown in Table 2, the porosity of the Sr-HA ceramics formed by cold isostatic pressing was obviously lower than that formed by dry pressing. During the process of the external electric field polarisation, part of the electric field would be exerted to the position of the pores of the Sr-HA ceramics. Both the stress concentration and electric field concentration caused by the pores would hinder the domain wall movement and the directional arrangement of the space charges, greatly reducing the polarisation efficiency and the remnant polarisation intensity of the ceramics. At the same time, the porosity of the Sr-HA ceramics obtained here was more than 25 %, the coercive electric field intensity of the Sr-HA ceramics obtained by cold isostatic pressing varied from 0.0313 $KV \cdot mm^{-1}$ to 0.3184 $KV \cdot mm^{-1}$, while that obtained by dry pressing changed from 0.0432 $KV \cdot mm^{-1}$ to 0.3209 $KV \cdot mm^{-1}$. The required coercive electric field increased with an increase in the porosity, which was consistent with the results of Zeng [25] and Zhang et al. [26]. Moreover, the dense hydroxyapatite ceramic has a hexagonal phase structure, the increase in the porosity would destroy its original hexagonal crystal structure and lead to a decrease in the remnant polarisation. From the above discussion, we can see that that the ferroelectric properties of hydroxyapatite ceramics could be improved by selecting proper ion doping ions and increasing the density of the samples.

CONCLUSIONS

Strontium-doped hydroxyapatite ceramics were successfully synthesised at low temperatures. The crystal structure, phase composition and ferroelectric properties of the strontium-doped hydroxyapatite ceramics changed with the Sr^{2+} ions doping concentration. When the Sr^{2+} doping contents were ≤ 15 mol. %, the lattice parameters a and c increased, but the crystallinity decreased with an increase in the Sr^{2+} doping concentration. The decrease in the symmetry of the HA crystal structure and the increase in the electric dipole moment caused by the Sr^{2+} doping increased the ferroelectric characteristic parameters and enhanced the ferroelectric properties of Sr-HA ceramics. Meanwhile, the ferroelectric properties of the Sr-HA ceramics were also affected by their porosity. The Sr-HA ceramics formed by cold isostatic pressing showed an improved ferroelectric performance when compared with the samples formed by simple dry pressing.

Acknowledgements

This work was supported by the National Natural Science Foundation of China (No. 51372182).

REFERENCES

1. Namdev M, Govinda K. (2017): Piezoelectric material – a promising approach for bone and cartilage regeneration. *Medical Hypotheses*, 108, 10-16. Doi: 10.1016/j.mehy.2017.07.021
2. G. S, Gobi Saravanan K, P. V, et al. (2021): Hydroxyapatite– barium/strontium titanate composite coatings for better mechanical, corrosion and biological performance. *Materials Today: Proceedings, 44*, 3618-3621. Doi: 10.1016/j.matpr.2020.09.758
3. Du M-Z, Chen J-D, Liu K-H, et al. (2021): Recent advances in biomedical engineering of nano-hydroxyapatite including dentistry, cancer treatment and bone repair. *Composites Part B: Engineering, 215*, 108790. Doi: 10.1016/j.compositesb.2021.108790
4. Nowsheen G, Archana B-L. (2022): Piezoelectric polymeric scaffold materials as biomechanical cellular stimuli to enhance tissue regeneration. *Materials Today Communications, 31*, 103491. Doi: 10.1016/j.mtcomm.2022.103491
5. Feng J-Q, Yuan H-P, Zhang X-D. (1997): Promotion of osteogenesis by a piezoelectric biological ceramic. *Biomaterials, 18*(23), 1531-1534. doi: 10.1016/S0142-9612(97)80004-X
6. Jiao H, Zhao K, Ma L, et al. (2017): Preparation and characterization of $BaTiO_3$/HA nanocomposite materials by hydrothermal synthesis. *Journal of Alloys and Compounds, 693*, 221-225. Doi: 10.1016/j.jallcom.2016.09.175
7. Bo Y-H. (1999): Study on polylactide/hydroxyapatite composites I. Synthesis and surface treatment of ultrafine hydroxyapatite. J*ournal of Sun Yat-sen University: Natural Science Edition*, 03,44-48.

8. Daniel T, Rahul S. T, Liang-Yo Y, et al. (2016): Biofabrication of bone tissue: Approaches, challenges and translation for bone regeneration. *Biomaterials, 83,* 363-382. Doi: 10.1016/j.biomaterials.2016.01.024
9. Liu T-T, Jin M-Q, Zhang Y-Z, et al. (2021): $K^{+}/Sr^{2+}/Na^{+}$ triple-doped hydroxyapatites/gelma composite hydrogel scaffold for the repair of bone defects. *Ceramics International, 47*(21), 30929-30937. Doi: 10.1016/j.ceramint.2021.07.277
10. Edward O'N, Guleid A, Leila D, et al. (2018): The roles of ions on bone regeneration. *Drug Discovery Today, 23*(4), 879-890. doi: 10.1016/j.drudis.2018.01.049
11. Ressler A., Žužić A., Ivanišević I., Kamboj N., Ivanković H. (2021): Ionic substituted hydroxyapatite for bone regeneration applications: A review. *Open Ceramics, 6,* 100122. Doi: 10.1016/j.oceram.2021.100122
12. Delannoy P. H., Bazot D., Marie P. J. (2002). Long-term treatment with strontium ranelate increases vertebral bone mass without deleterious effect in mice. *Metabolism-Clinical and Experimental, 51*(7), 906-911.Doi: 10.1053/meta.2002.33360
13. Reem Al-Wafi. (2016): Ferroelectric properties of sr doped hydroxyapatite bioceramics for biotechnological applications. *Journal of Alloys and Compounds, 689*, 169-173. Doi: 10.1016/j.jallcom.2016.07.285
14. M. S. A. (2016): Nanostructure hydroxyapatite based ceramics by sol gel method. *Journal of Alloys and Compounds, 661*, 251-256. Doi: 10.1016/j.jallcom.2015.11.045
15. Zhang H-Q, Brian W. D. (2011): Morphology and structural characteristics of hydroxyapatite whiskers: Effect of the initial Ca concentration, Ca/P ratio and pH. *Acta Biomaterialia, 7*(7), 2960-2968. Doi: 10.1016/j.actbio.2011.03.020
16. Wen J, Zhang H-Q, Fu L-W, et al. (2014): Composition, structure and antibacterial properties of magnesium, zinc, strontium ion doped HA. *Rare Metal Materials and Engineering. 0*(S1), 59-62.
17. Geng Z, Cui Z-D, Li Z-Y, et al. (2015): Synthesis, characterization and the formation mechanism of magnesium- and strontium-substituted hydroxyapatite. *Journal of Materials Chemistry B, 3*(18), 3738-3746. Doi: 10.1039/C4TB02148G
18. S Baravelli, A Bigi, A Ripamonti, et al. (1984): Thermal behavior of bone and synthetic hydroxyapatites submitted to magnesium interaction in aqueous medium. *Journal of Inorganic Biochemistry, 20*(1), 1-12. Doi: 10.1016/0162-0134(84)80001-X
19. Li Z.Y, Lam W.M, Yang C, et al. (2007): Chemical composition, crystal size and lattice structural changes after incorporation of strontium into biomimetic apatite. *Biomaterials, 28*(7), 1452-1460. Doi: 10. 1016/j.biomaterials.2006.11.001
20. Zhang H-Q, Zhang M. (2011):Characterization and thermal behavior of calcium deficient hydroxyapatite whiskers with various Ca/P ratios. *Materials Chemistry and Physics, 126*(3), 642-648. Doi: 10.1016/j.matchemphys.2010.12.067
21. Joice T, Erico Rodrigues D, Jean-Guillaume E, et al. (2009): The structure of strontium-doped hydroxyapatite: An experimental and theoretical study. *Physical Chemistry Chemical Physics, 11*(3), 568-577. Doi: 10.1039/B802841A
22. A Bigi, G Falini, E Foresti, et al. (1993): Magnesium influence on hydroxyapatite crystallization. *Journal of Inorganic Biochemistry, 49*(1), 69-78. doi:10.1016/0162-0134 (93)80049-F
23. Liu J. (2018): Preparation, characterization and computational simulation of Sr^{2+}/Eu^{3+} Co-doped hydroxyapatite. Master's degree thesis. Shaanxi University of Science and Technology. Shanxi,China.
24. Sun J-P. (2014): First principles study of structures and characteristics of the interfaces between titanium and hydroxyapatite under aqueous solution. Doctoral thesis. Harbin Institute of Technology. Harbin, China.
25. Zeng T, Bai Y, Shen X-X, et al. (2014): Study on mechanical and ferroelectric properties of porous PZT95/5 ferroelectric ceramics. *Journal of Inorganic Materials, 29*(7), 758-762.
26. Zhang Y, Roscow J, Lewis R, et al. (2018): Understanding the effect of porosity on the polarisation-field response of ferroelectric materials. *Acta Materialia, 154*, 100-112. Doi: 10.1016/j.actamat.2018.05.007
27. Padurariu C, Padurariu L, Curecheriu L, et al. (2017): Role of the pore interconnectivity on the dielectric, switching and tunability properties of PZTN ceramics. *Ceramics International, 43*(7), 5767-5773.Doi: 10.1016/j.ceramint.2017.01.123
28. Felicia G, Leontin P, Mirela A, et al. (2017): Porosity-dependent properties of Nb-doped $Pb(Zr,Ti)O_3$ ceramics. *Journal of the American Ceramic Society, 100*(2), 647-658. Doi: 10.1111/jace.14587